Stapp Car Crash Journal, Vol. 60 (November 2016), pp. 11-24

2016-02

The Effect of Rib Shape on Stiffness

Sven A. Holcombe[1,2], Stewart C. Wang[2], James B. Grotberg[1]
[1] Department of Biomedical Engineering, University of Michigan
[2] International Center for Automotive Medicine, University of Michigan

ABSTRACT – This study investigates the isolated effect of rib shape on the mechanical characteristics of ribs subjected to multiple forms of loading. It aims to measure the variation in stiffness due to shape that is seen throughout the population and, in particular, provide a tool for researchers to better understand the influence of shape on resulting stiffness.

A previously published six-parameter shape model of the central axis of human ribs was used. It has been shown to accurately model the overall rib path using intrinsic geometric properties such as size, aspect ratio, and skewness, through shapes based on logarithmic spirals with high curvature continuity. In this study the model was fitted to 19,500 ribs from 989 adult female and male CT scans having demographic distributions matching the US adult population. Mechanical loading was simulated through a simplified finite element model aimed at isolating rib shape from other factors influencing mechanical response. Four loading scenarios were used representing idealized free and constrained loading conditions in axial (body-anterior) and lateral directions. Characteristic rib stiffness and maximum stress location were tracked as simulation output measures.

Regression models of rib stiffness found that all shape model parameters added information when predicting stiffness under each loading condition, with their linear combination able to account for 95% of the population stiffness variation due to shape in mid-level ribs for free axial loading, and 92%–98% in other conditions. Full regression models including interactive terms explained up to 99% of population variability. Results allow researchers to better evaluate the differences in stiffness results that are obtained from physical testing by providing a framework with which to explain variation due to rib shape.

KEYWORDS – Ribs, Rib stiffness, Rib shape, Biomechanics, Thoracic injury, Population, Spiral

INTRODUCTION

The thoracic skeleton plays a vital role in protecting occupants in motor vehicle crashes (MVCs), and it is also one of the most frequently injured segments of the body. Within the thorax rib fractures are the most common skeletal injuries in MVCs (Kent 2008, Abdulrahman 2013), and are found in multiple crash configurations including those involving frontal, side, and oblique impact and loading directions. Rib fractures can cause physiological complications including pain and reduced vital reserve, and are often accompanied by associated thoracic and abdominal injuries making their presence indicative of the severity of injury to the chest (Livingston 2004, Bulger 2000, Holcomb 2003, Bergeron 2003).

Thoracic injury criteria are typically related to measures of chest compression. In most cases this deflection is measured at the sternum and thus is most sensitive to body-anterior loading similar to that experienced by occupants in frontal impacts (for summary see Kent and Patrie, 2005). In lateral impact scenarios, however, the position of maximum deflection of the rib cage varied from lateral regions to antero-lateral regions depending on impact conditions including the position of the arms and the size and shape of the impacting surface (Song 2009). Similarly, deformation modes of the chest vary between lateral and oblique impacts (Shaw 2006) indicating that ribs experience deflection initiated from a range of body directions depending on impact scenario. Furthermore, the magnitude of lateral rib deflection during loading has been shown to be a good indicator of rib damage (Song 2009).

The biomechanical response of the chest and ribs to loading has been investigated at multiple scales

Address correspondence to Sven Holcombe, Department of Biomedical Engineering, University of Michigan. Electronic mail: svenho@umich.edu

ranging from full body or thorax testing to individual component or material tests. At each scale, some degree of variability in response comes from the individual variation between subjects or components being tested. At the component level describing an isolated rib's response to loading, the overall structural stiffness comes from the accumulated effects from local bone material makeup (see, for example, Stein 1976, Cormier 2005, Agnew 2013), localized geometric properties such as rib cross-sectional shape and regional cortical bone thickness (Stitzel 2003, Shi 2014, Takahashi 1966), as well as overall geometric shape and size properties (Shi 2014, Weaver 2014, Wang 2016).

A number of experimental studies have utilized whole ribs excised from post-mortem human subjects (PMHS). Charpail et al. (2005) established a testing framework that simulated the anterior-posterior loading seen in frontal impacts using 4th to 9th ribs from five subjects, including a representation of stiffness in terms of the force vs. displacement at the loaded end. Kindig et al. (2011) tested 2nd to 10th ribs from three subjects, describing average differences in stiffness and mechanical response by rib level, with 2nd ribs being 3 to 4 times stiffer than other levels. Agnew et al. (2015) applied dynamic loading using an impactor to 140 ribs from 70 individuals across a full age spectrum including children. That study focused on age trends, and results showed a decrease in rib stiffness with age, as well as a decrease in the displacement that ribs underwent before fracture. In each outcome substantial variation was seen across the tested samples, with age explaining only 13.8% of the variation in stiffness. A single shape parameter of rib aspect ratio (height in the local plane divided by end-to-end span) did not have strong correlations with response, but the authors suggested that a more complete characterization of shape and curvature may provide more insight.

A parametric model of in-plane human rib geometry has been developed that accurately quantifies overall rib shape (Holcombe 2016). Its six parameters act both as measures of overall size and shape, while also providing a mechanism to fully create a rib's shape from the parameters alone. It uses intrinsic geometric properties of the rib such as size and aspect ratio in its parameterization, meaning that ribs rebuilt using average parameters reflect the average intrinsic geometry from their underlying group of rib shapes.

The goal of this study is to extend the utility of the six-parameter rib shape model from Holcombe et al. (2016) to include the relative influence of each of its parameters (or combinations thereof) on the structural stiffness of rib shapes. Doing so enables researchers to better stratify ribs that are used in physical tests by accounting for variation in stiffness outcomes that come as a result of different rib sizes and shapes across experimental subjects. In this study we target a loading setup used in previous experiments representing nominally body-anterior loading, as well as exploring other simplified loading conditions that might be included in future tests to represent different loading situations.

METHODS

Rib shape model

All overall rib geometry in this study was represented using a six-parameter shape model that characterizes the central axis of human ribs with a pair of logarithmic spirals (Holcombe 2016). In this study the terms distal and proximal (to the spine) will be used to refer to directions along ribs. A depiction of the model and its parameters is provided in Figure 1. Four of these parameters are intrinsic geometric properties of a rib's in-plane size and shape. As shown in Figure 1, the S_x parameter sets the end-to-end rib size, while the rib's peak is given (normalized by S_x) by the parameter pair [X_{Pk},Y_{Pk}]. Together, these describe a rib's aspect ratio ($1/Y_{Pk}$) and "skewness", with lower X_{Pk} values moving the rib peak closer to the proximal end. The φ_{pia} parameter specifies the inner angle at the proximal (to the spine) end of the rib, while B_p and B_d are logarithmic spiral constants. For full shape derivation and discussion of the model, the reader is directed to Holcombe et al. (2016).

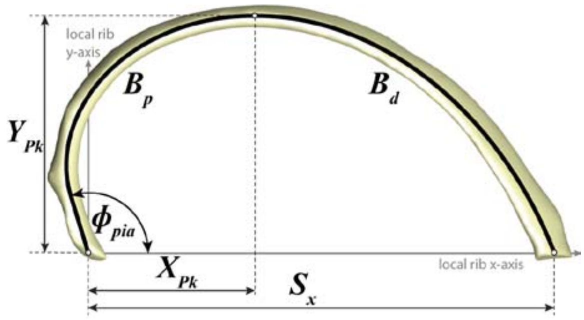

Figure 1. Rib shape model with one size parameter (S_x), parameters for the rib peak position (X_{Pk},Y_{Pk}, normalized by S_x) giving skewness and aspect ratio, the initial inner angle at the proximal rib end (ϕ_{pia}), and proximal and distal spiral constants (B_p,B_d). Parameters fully define two logarithmic spirals that meet with zero slope at the rib's peak.

Study population and individual ribs

The rib shape model was fitted to over 19,500 ribs from a population of 989 live adult subjects[1] (491 females, 498 males) in the International Center for Automotive Medicine (ICAM) CT scan database. Subjects underwent a chest and/or abdomen CT scan during trauma treatment and diagnosis. Axial scan resolutions were between 0.54–0.98 mm, with a median of 0.70 mm, and slice spacing ranged from 0.625–5.0 mm with most acquired at 1.25 mm. Each rib geometry is given by an optimized fit of rib shape model parameters to the centroidal path of ribs, which are specified by the sequence of centroids to 2D cross-sections along the rib as described in Holcombe et. al (2016). Only non-fractured ribs were considered for this study. Subjects were between 20 and 98 years of age at the time of scan, with a mean age of 48 and 52 years for males and females, respectively. Population distributions of subject heights and weights compared well to a CDC American adult reference population (Fryar 2012), with differences in height and weight at 5th, 25th, 50th, 75th, and 95th percentiles below 0.2 standard deviations for all groups except for 95th percentile females who were 0.3 and 0.4 standard deviations taller and heavier than their comparison CDC cohort, respectively.

FE simulation setup

A finite element (FE) modeling system was set up in LS-Dyna (LSTC, Livermore, CA) for any given rib's in-plane shape defined by values from the six-parameter shape model. The goal of the system was to retain sensitivity to overall rib shape – which was modeled directly – by approximating all other aspects of geometry and material makeup through a highly simplified representation. Each given rib shape was discretized to a 100-by-12 cylindrical mesh using quad-shell elements at a mid-surface radius of 5 mm. A simple linear elastic material model was used (ρ = 2000 kg/m^3, E = 11GPa, ν = 0.3, Kemper et al., 2007; Granik and Stein, 1973; Li et al., 2010), and the cortical shell thickness was set to 1 mm. Rib cross section and material properties were held constant along the rib and equivalent for all input so as to isolate the changes in mechanical behavior driven directly by changes in overall rib shape.

Four simulation configurations were used representing idealized loading from free and constrained displacement of the rib in both axial (along the rib's local x-axis) and lateral (along the rib's local y-axis) directions as depicted in Figure 2. A nodal rigid body was formed from the circle of nodes at each end of the rib, and point loads and constraints applied to those bodies' centers of mass (i.e., the distal and proximal end points of the rib central axis).

In axial loading conditions rib ends were constrained against out-of-plane rotations (but free to rotate in-plane). Only translation of the distal end along the rib's local x-axis was permitted and nodal displacement was applied in this direction. For the constrained axial loading condition, a rigid and frictionless fixed-wall

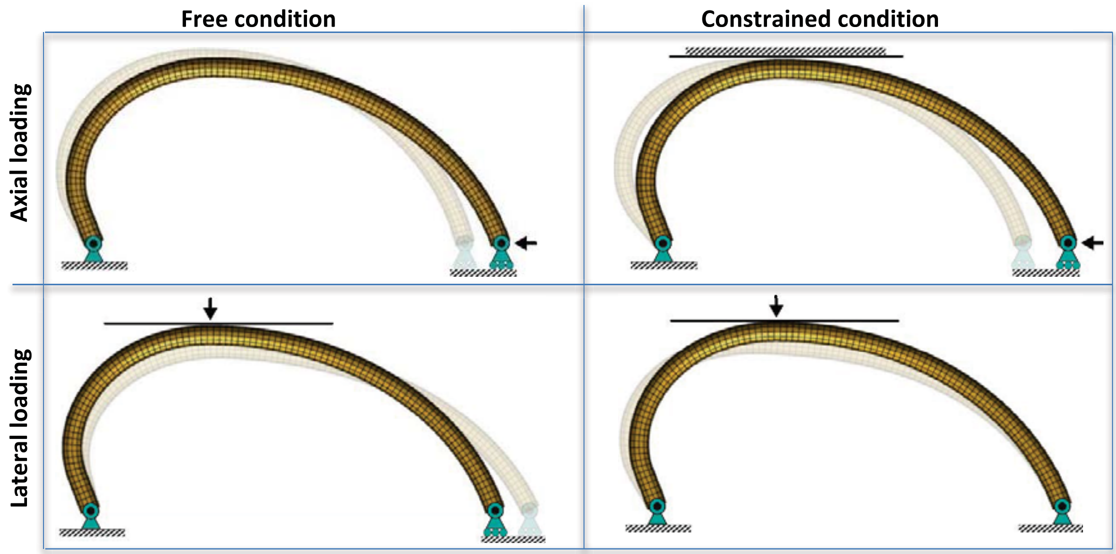

Figure 2. Four simulation loading conditions

[1] Image data obtained under IRB approval [HUM00041441]

contact surface was added immediately above the top-most node on the rib, limiting upwards displacement during bending. In the lateral loading conditions, the rigid wall was displaced downwards causing rib displacement in the local y-direction. For the free lateral condition, the distal end was free to translate along the x-axis, and in the constrained lateral loading condition both rib ends were constrained against all translation in similar fashion to a three-point bending configuration.

Loading in all cases was applied in a quasi-static fashion over a 100 ms simulation time. To minimize dynamic effects at force onset, nodal velocity was ramped to provide gradual displacement as illustrated in Figure 3. Resulting force measures were checked for inertial artifacts such as ringing or settling time (via test simulations with abruptly ceased displacements) and were found to be consistent with the intended condition of quasi-static loading.

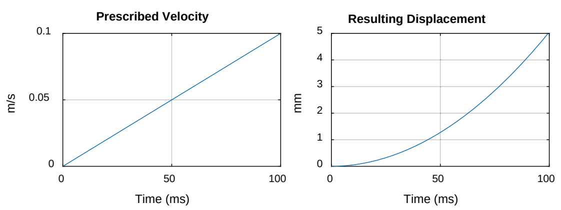

Figure 3: Ramped velocity for gradual nodal displacement.

Stiffness calculation

Rib stiffness was defined by the initial slope of the force vs. displacement relationship during loading. In axial loading, the reaction force (F_x) and displacement (Δ_x) in the x-direction at the distal rib end up to $\Delta_x = 5$ mm were used. For lateral loading, the rigid wall reaction force (F_y) and vertical displacement (Δ_y) up to 2 mm were used. To account for any non-linearity in the force vs. displacement relationship, a least-squares fit to the following equation was found:

$$F = a\Delta^2 + K\Delta$$

In all cases the mean error from this fit was less than 0.3% of the reaction force at $\Delta_x = 5$ mm or $\Delta_y = 2$ mm for the axial and lateral conditions, respectively. The linear constant K provides the initial slope of the fit, and therefore the characteristic stiffness in N/mm. Figure 4 shows this graphically for the constrained axial condition, which offered the most non-linear response of the four conditions.

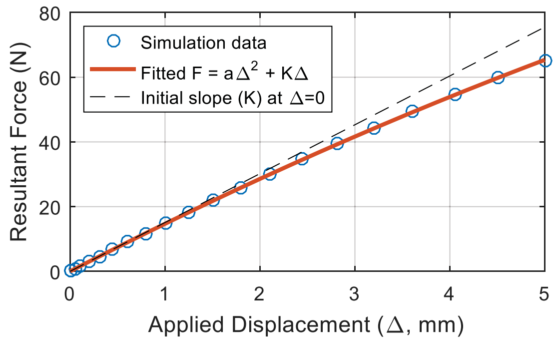

Figure 4: Force vs. displacement curve under constrained axial loading with stiffness determined by the initial slope.

Along with stiffness in each loading configuration, the additional outcome of percentile location along the rib of the maximum von Mises stress at 5 mm (axial) or 2 mm (lateral) displacement was measured.

Model validation

Rib stiffness to static loading will be influenced primarily by the combined contributions from overall rib shape, local cross-sectional geometry, regional cortical bone thickness, and the regional material properties of the cortical and trabecular bone. The aim of the FE modeling scheme in this study is to approximate the combined contributions from all factors other than overall shape, yet remain sensitive to the effect on stiffness produced by changes in that shape.

As validation that the model adequately combined these influencing parameters to produce realistic stiffness magnitudes, a comparison was made between magnitudes found from experimental tests on a population performed by Agnew et. al (2015) and computational tests using our methodology (Holcombe 2016). For consistency between ribs being compared, only adults 20–70 years and ribs 4–8 were included from either study, shown together in Figure 5. Student's t-tests using both raw stiffness values and log transformed stiffness values each showed no significant difference between population means ($t(1160)=1.28$, $p=0.2$ for raw, $t=-0.7$, $p=0.48$ for log transformed). Furthermore, strain patterns were consistent with quasi-static tests from a smaller population of 3 individuals (Kindig 2011) whereby higher positive (external surface) and negative (internal surface) strain magnitudes were seen in lateral rib regions than in proximal or distal rib regions.

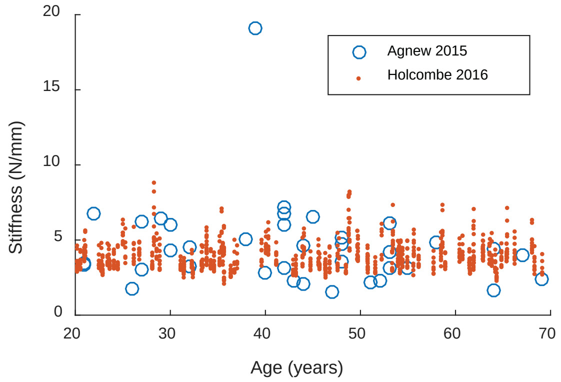

Figure 5: Stiffness under axial loading simulated from ribs of 100 individuals (Holcombe 2016) who form part of this study and from physical tests of ribs from 70 individuals (Agnew 2015).

RESULTS

All individuals' ribs were subjected to each of the four simulated loading conditions. Stiffness to each loading type was recorded, along with the position and value of maximum von Mises stress along each rib during deformation.

Overall stiffness distributions

Overall stiffness results by rib in general followed a log-normal distribution, with the stiffness of shorter 1st and 12th ribs in axial loading, for example, being considerably higher than other levels. Overall trends by rib level in each condition are given in Figure 6 using log transformed stiffness values. Here it can be seen that stiffness was higher in lateral loading conditions, and higher in each constrained condition compared to free conditions. Stiffness of the longer mid-level ribs were generally lower than upper- or lower-level ribs.

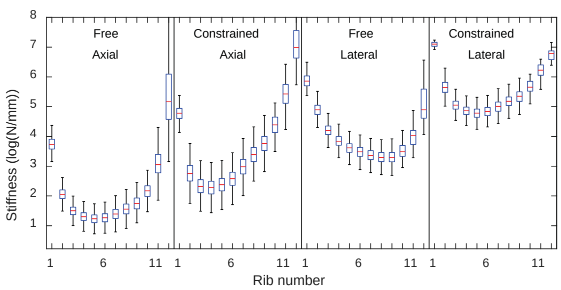

Figure 6: Log transformed stiffness to each loading condition by rib level.

Predicting stiffness by shape parameters

Using pooled data from mid-level ribs 4–8, the ability of the rib shape parameters to predict resulting stiffness variation was tested. This mid-level subset of ribs was used in order to correspond to previous testing selection criteria (Agnew 2015). These rib levels also exhibit an overall similar topology and size (8th ribs are 20%, 12%, 6%, and 1% longer than 4th through 7th ribs, respectively; Holcombe 2016), and their combined outcome stiffness results formed normal distributions. Linear regression was performed using log transformed stiffness to a given condition as the response variable, and each of the rib shape model parameters as predictor variables. For each analysis, a training set of 60% of the ribs was randomly selected and the remaining 40% were used to test the resulting predictions. In all cases all coefficients were highly significant ($p<0.001$) except for X_{Pk} in free axial loading ($p=0.057$) and B_p in free lateral loading ($p=0.002$). Coefficients for each parameter in each loading condition along with predictive model performance for each training and testing sample set are provided in Table 1. Repeated analyses using different randomly selected training sets provided similar coefficients and performance.

Table 1: Linear regression coefficients using the rib shape model parameters to predict stiffness (ln(N/mm)) to loading of mid-level ribs. Training/test data consisted of a random 60/40 selection of rib observations.

	Free Axial	Constr. Axial	Free Lateral	Constr. Lateral
Constant	6.49	2.23	7.37	9.94
S_x (mm)	-0.0141	-0.0126	-0.0141	-0.0123
Y_{Pk} (mm/S_x)	-5.1644	-9.6116	-0.1280	-4.4487
X_{Pk} (mm/S_x)	-0.0560	4.9017	-3.3727	1.7148
φ_{pia} (deg)	-0.0008	-0.0083	-0.0004	-0.0083
B_p	0.0291	0.6419	-0.0130	0.6101
B_d	0.0563	0.1061	-0.0116	0.0459
R^2 (train)	94.9%	97.0%	98.1%	93.3%
R^2 (test)	95.5%	96.9%	97.6%	92.8%

Stratified rib shape by stiffness and level

Ribs from all subjects were stratified by their stiffness under each individual loading condition, and separated into groups from least to most stiff. Averages for each of the six rib shape parameters were calculated from within groups, and are provided in Tables A1 through A4. These data are passed directly to the rib shape model to produce typical rib shapes that are softest (below 10th percentile), average (45th to 55th percentile), and stiffest (above 90th percentile) under a given loading condition as shown in Figures 7 and 8.

In free axial loading (Figure 7, top), stiffer ribs tend to have shorter end-to-end spans (lower S_x parameter), and greater aspect ratio (lower Y_{Pk}). These trends are reflected by the coefficients for S_x and Y_{Pk} from Table 1 both being negative in sign. Under constrained axial loading (Figure 8, bottom), stiffer ribs had similarly high aspect ratio (lower Y_{Pk}), but also tended to be initially directed more anteriorly (lower φ_{pia}) and had less skewness whereby their peak (X_{Pk}) was shifted towards the middle of the rib. Overall size, which was seen to be negatively associated with stiffness in the pooled regression model, was generally similar between stratified rib groups for each rib level.

Figure 8 shows the stiffest and softest rib shapes under free lateral (top), and constrained lateral loading (bottom). In both lateral loading conditions rib span (S_x) is a primary factor driving stiffness, however in constrained lateral loading, other factors that serve to reduce the overall arc length of a rib tend to produce the stiffest response.

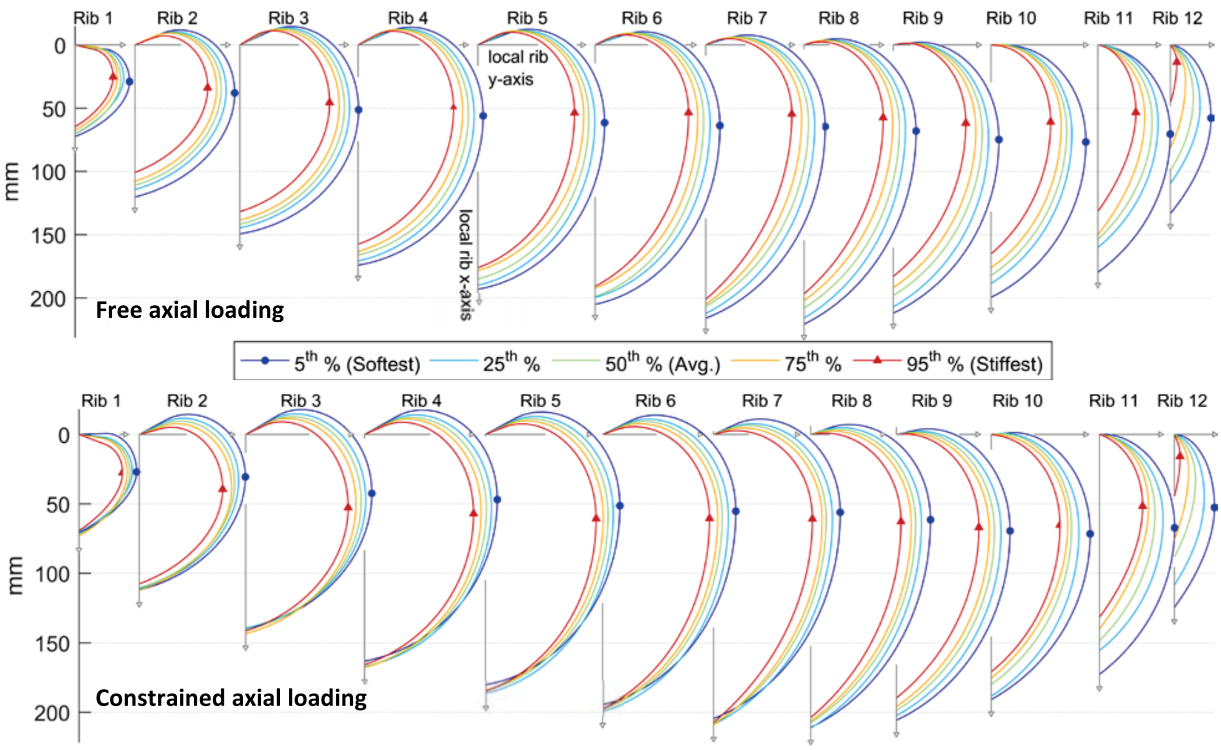

Figure 7. Typical rib shapes with low, medium, and high stiffness under free or constrained axial displacement

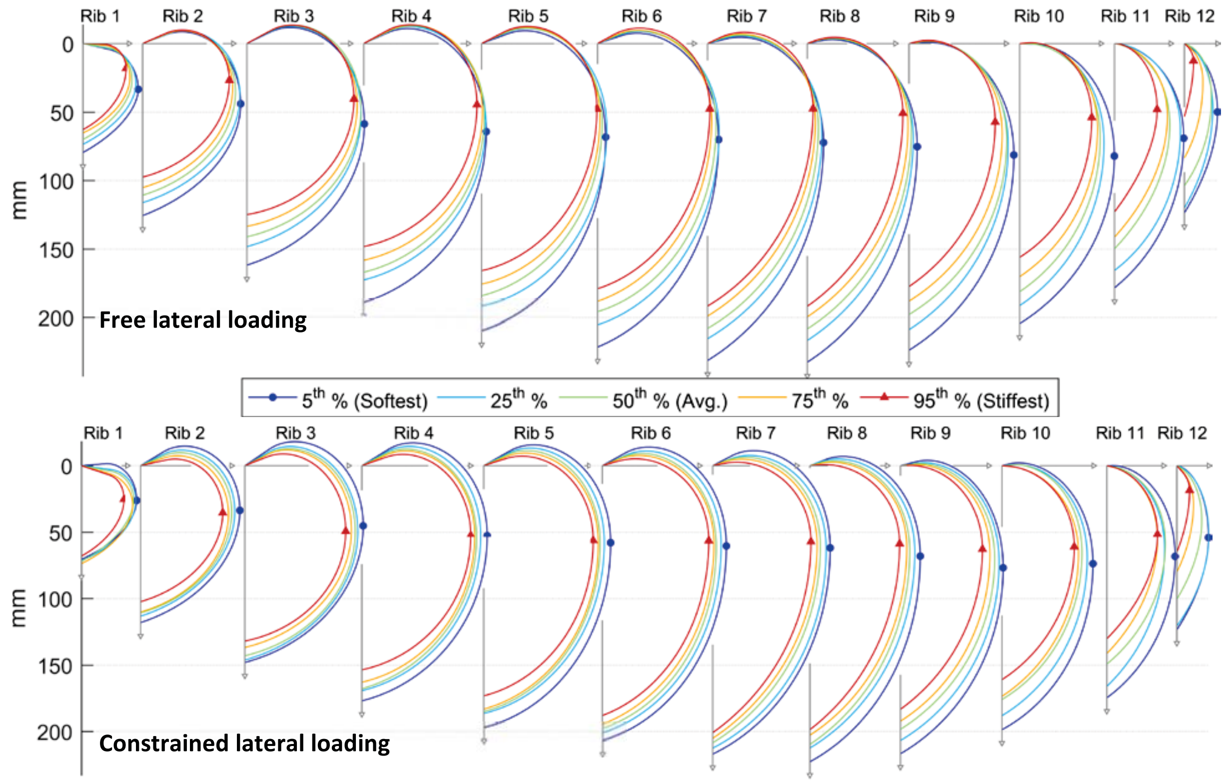

Figure 8. Typical rib shapes with low, medium, and high stiffness under free or constrained lateral displacement

Stress distribution by loading

Exemplar von Mises stress distributions at 5 mm or 2 mm displacement in each of the loading conditions are shown for typical 6th ribs in Figure 9. Maximum stress location was determined for each simulated rib at discrete element locations arranged from the proximal or vertebral end (0% along the rib arc length) to the distal end (100% along the arc length). For loading configurations with a rigid wall contact, the local stress concentration at the contact site was ignored when tracking the maximum stress location, and only local maxima at other regions of the rib were considered.

Across the full population, the maximum stress location under free axial loading was invariably within a short distance (2% of overall rib length) from the apex of the rib. Due to the differing shapes for each rib level, this was between 40%–55% of the arc length for ribs 2 and 3, and occurred progressively earlier for successive rib levels up to the 8th rib, which had its apex located between 35–45% along its length. Under constrained axial loading the location of maximal stress ranged from 20–26% along the rib's length (rib 2) to 16–19% along the rib's length (rib 9). Constrained lateral loading produced stress distributions similar to those seen in constrained axial loading, with a concentration due to contact under the loading wall, and a maximum stress location towards the posteriorly extending rib region. Free lateral loading stress was dominated by the region in contact with the moving wall.

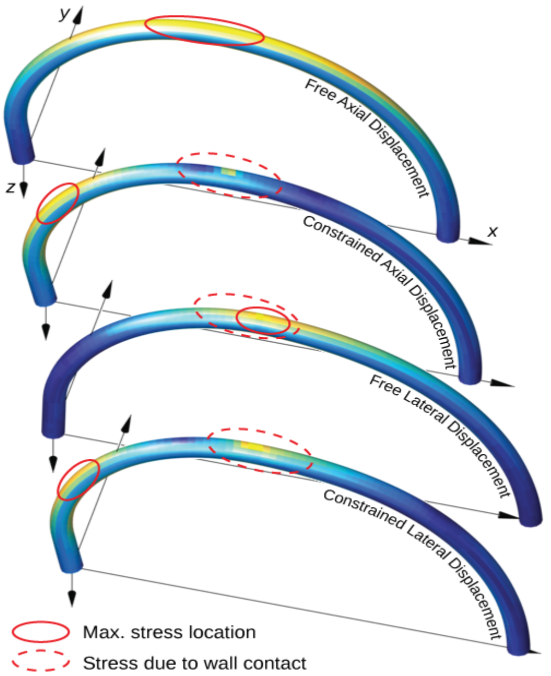

Figure 9: von Mises stress distribution at maximal displacement in each condition for typical 6th ribs. Wall contact produced a local stress concentration, so maximum stress locations were considered only in non-contact regions.

DISCUSSION

Simulated mechanical loading was performed for a large population of rib shapes from live adults extracted from CT image data. The subject group was chosen so as to adequately represent the breadth of demographics seen throughout the population. An efficient parametric model produced a simplified representation of the overall rib shape, and mechanical loading was simulated for each rib. Results in terms of stiffness to loading were collected in multiple loading conditions. Results showed the typical rib shapes that are stiffest or softest under different loading conditions, and found that variation in stiffness due to shape variability could be predicted with considerable accuracy directly from the underlying shape model parameters.

Loading conditions

The free axial loading condition used in this study was chosen to match the framework set forth in Charpail et al. (2005) which has since been adopted in multiple experimental studies (Kindig 2011, Li 2010, Agnew 2015). While not duplicating boundary conditions from an intact human thorax, this framework aims to model the forces that are applied to ribs during frontal impact loading. In this study we have further idealized the loading conditions at the fixation points of either rib end. The experimental procedures include fixation of the rib to loading apparatus using a potting cup around each end. This potting affects the overall response to some degree by reinforcing rib ends and effectively reducing the deformable length of the rib. Here we have chosen to idealize the rib end fixations by a single ring of rigid nodes and maximize the deformable rib length, rather than incorporate an added variable representing the length of the potted region for each rib.

In real-world MVCs ribs are loaded (and injuries incurred) through a variety of impact scenarios, and the single framework represented by free axial loading is unlikely to cover the breadth of these conditions. In lateral and oblique impacts to PMHS subjects, a variety of chest deformation modes are seen (Shaw et al. 2006, Pintar et al. 2007, Baudrit et al. 2014). These include deformation in primarily lateral directions, antero-lateral directions, and with varying degrees of sternal deflection. In this study three additional loading setups were considered that approximate rib loading that might be experienced in such configurations. In each case the simulated boundary conditions once again do not duplicate boundary conditions from an intact human thorax, but have been chosen based primarily for their simplicity and their ease of implementation during experiments.

As a modification of the free axial loading condition (designed to represent an anterior-only body load), the constrained axial loading represents a primarily body-anterior load with a lateral component sufficient to prevent lateral displacement (or y-displacement in the local rib plane) of ribs during deformation. The rigid wall component is expected to require only minor modification of the Charpail testing framework to include an added rigid barrier placed above the rib in its initially unloaded position. Agnew et. al (2015) found variation in the extent of y-displacement during loading that was not clearly related to investigated shape or demographic factors. As such, the conditions of constrained axial loading may be beneficial and serve to remove this variation.

The constrained lateral loading condition represents a primarily lateral load to the body, but with a sufficient anterior component to prevent anterior rib displacement. The free lateral loading setup is less likely to be experienced *in vivo* due to the presence of costal cartilage and the sternum, but it tests a rib that is loaded from a lateral direction but experiences no resistance to displacement of its sternal end. A primary criteria behind the choice of each condition was an ability for that loading condition to be reproduced experimentally.

Each loading scenario measured stiffness to a differing set of loading conditions, however there were similarities between conditions and they were not fully independent. Log-transformed stiffness results from free axial displacement of rib 6 could explain 57.5% of the stiffness variation under constrained axial displacement (using adjusted r-squared values) and 54.2% of stiffness variation in constrained lateral displacement. Constrained axial and constrained lateral displacement stiffness values were the most strongly correlated, with the latter explaining 65.2% of variation in the former. Free lateral displacement was correlated with constrained axial displacement stiffness (adjusted r-squared of 21%) but not well correlated with stiffness in free axial displacement (adjusted r-squared less than 1%).

Stress location variation

Results from this study suggest that overall shape does influence the position of maximum stress as a function of overall arc length, however this position varies across the population by around 10%–15% of the rib's length, and primarily tracks key locations such as the rib peak. In free axial loading, stress is distributed more evenly over a large portion of the rib than in the two constrained conditions where a localized stress concentration is present near the posterior arch. For context, Agnew et. al. (2015) specified rib positions categorically as posterior, lateral, and anterior, and found fractures after axial loading to occur in each zone (but with the anterior and lateral locations most common), making fracture distribution less localized than is seen in the maximum stress locations here. These results suggest that the actual fracture site may be more dependent on local factors such as regional material or cortical thickness properties than it is on overall rib shape.

Cross-sectional influence on stiffness

The FE modeling setup used in this study is informed by linear beam theory wherein beam stiffness scales with cross-sectional inertial moment. A parameter study with varying wall thickness between 0.1 and 1.0 mm (i.e., wall thickness much thinner than overall section size) confirmed this relationship, with stiffness in free axial loading varying close to linearly at 4 N/mm per 1 mm shell thickness change within this range. The shell element formulation was chosen (rather than 1D beam) for its relative ease when extracting element data from LS-Dyna ASCII output databases in an automated fashion. Similarly to the changes seen by shell thickness adjustment, modification of the Young's modulus material property within an order of magnitude corresponded to linear changes in overall stiffness at a rate of around 0.38 N/mm per 1 GPa.

Representativeness of average rib shapes

An important factor to consider when generating new rib geometry from statistical operations on parameter values is whether the resultant rib shapes are indeed representative of the underlying group. One benefit of the shape model used here is its reliance on intrinsic geometric properties (size, aspect ratio, etc.). This guarantees that the average shape from within any group will have exactly the average size, aspect ratio, skewness, and inner angle of all of its constituent ribs. Inspection of distributions in shape parameter values (including the spiral shape constants) from individual ribs or from the pooled set of mid-level ribs showed strongly normal distributions. These properties of the shape model and its parameters' distributions give confidence that the averaging approach generates rib shapes that are typical of the population. This result is illustrated in Figure 10, which shows the average ribs computed from the stiffest and softest groups of 6th ribs under free axial loading (i.e., those first seen in Figure 7). Here it can be seen that even with ribs from the extreme ends in terms of stiffness response, each average shape gives an accurate representation of typical ribs in each underlying group.

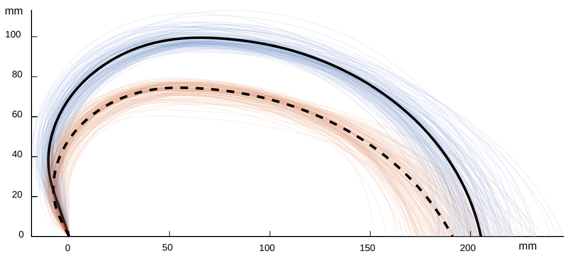

Figure 10: Rib 6 shapes of the stiffest (dashed line) and softest (solid line) 10th percentile groups under free axial loading. Parameter-average ribs show good agreement with the constituent rib shapes from each underlying population.

Statistical models of stiffness by parameters

Each of the four regression models presented in Table 1 contain all six rib shape parameters as predictors. To assess the information content provided by different parameters both backwards selection and forwards selection models were calculated (using Akaike Information Criterion), and each resulted in this full inclusion of all shape parameters. This indicates that every shape parameter was informative in predicting output stiffness. When considering the relative importance of parameters, it was observed that the intrinsic geometric properties generally contributed most to the overall explanatory power. Separate linear models using just size and aspect ratio (S_x, Y_{Pk}) explained up to R^2=93% for free axial loading, and all four intrinsic parameters explained 90% of variation in constrained axial loading and 71% of variation in constrained lateral loading. Size and skewness (S_x, X_{Pk}) explained most of the variation in free lateral loading (98%). These results are reflected in the stratified rib shapes, which showed clearest differences between the groups of stiff or soft ribs in each of these identified parameters.

Within any given set of physical experiments whereby ribs are tested for their structural stiffness there will always be some degree of variability. Researchers are most often interested in identifying trends within this variation. Agnew et. al (2015), for example, assessed age as a predictor of mechanical response in free axial loading. Structural stiffness was seen to reduce with age at a rate of approximately -0.33 N/mm per decade, albeit with considerable variability having a pseudo-r-squared value of 13.8%. In that analysis rib shape itself was not controlled for other than in the selection of mid-level ribs. Rib aspect ratio (height in the local plane divided by span) was measured but not included in the age analysis as it alone did not have a strong correlation with stiffness. In that paper the authors suggested that a more sophisticated method of characterizing curvature of a rib may provide more insight. The intention for the current study is to offer that characterization through both the rib shape model parameters and the expected linear stiffness provided by the regression coefficients in Table 1. By fitting the shape model to each tested rib shape and calculating an expected linear stiffness, an additional predictive parameter could be added to analyses which would account for differences in stiffness between ribs due to their shape. Doing so might allow researchers to better control for the influence that overall shape has on their measured results, and would serve to clarify changes with other variables such as age.

Limitations and future work

This study is designed specifically to isolate changes in mechanics that are driven purely by overall rib shape, and this limitation should be taken into account when interpreting its results. For example, the authors do not intend this work to provide a reference for absolute stiffness or indeed the precise location of maximum stress seen when loading human ribs. Each of these outcomes rely on additional factors that have been deliberately excluded from this study's design. Further, the regression model performance measures do not suggest that 95% (for example) of all variation in stiffness from physical tests should be explicable using shape parameters alone. Instead, they suggest that of whatever variation in test results that are due to shape, these can be approximated to 95% accuracy using shape model parameters.

It is also important to acknowledge that the verification steps taken in this study have been done only through simulation. Using approximations for non-shape-related factors we have verified that overall stiffness values in axial loading match the distribution of those seen in physical testing, however no direct comparisons have been made between physical and simulated stiffness of identically shaped ribs.

In terms of overall shape, it should also be noted that the shape model used describes only the in-plane geometry of ribs. Ribs are known to also deviate from a fitted plane by up to 8% of a rib's end-to-end span (Kindig 2013). It would be expected that greater out-of-plane deviation would serve to reduce stiffness to a small degree in the loading conditions presented here, and determining the extent of this influence should be a focus of future work. Enhancement of the current model to include out-of-plane deviation of the rib centroidal path is likely to increase the predictive accuracy of the current study when comparing results to physical experiments.

Future efforts can also be directed at understanding the role that age and other demographic factors play in determining mechanical response of ribs to loading. Mechanical responses such as stiffness to loading are a physical aggregation of multiple different geometric and material factors. Age is known, for example, to affect a number of measures bone quality (see Boskey et. al 2010 for review) as well as overall rib stiffness (Agnew 2015). Analysis of the variation in rib shape parameters that are associated with demographics could be combined with results from the current study to investigate how potential changes in rib size and shape by demographics might affect the resulting stiffness of those ribs.

CONCLUSION

Ribs from a large population of live adults were characterized using a rib shape model fitted to geometry extracted from CT scans. The subject group was chosen so as to adequately represent the breadth of demographics seen throughout the population. Simulated loading under simplified conditions was applied in one loading scenario matching current experimental test procedures, and three modified scenarios for potential future testing. Results showed the typical rib shapes that would be stiffest or softest under each given loading condition. Linear regression was used to provide an expected stiffness to loading as a function of rib shape parameters. This model can be used in analysis of physical rib test results to help account for the effects of variation in overall rib shape on mechanical properties.

ACKNOWLEDGMENTS

The authors wish to thank Matthew Kindig for advice, data, and discussion regarding shape modeling and testing procedures.

REFERENCES

Agnew, A. M., Moorhouse, K., Kang, Y.-S. S., Donnelly, B. R., Pfefferle, K., Manning, A. X., Litsky, A. S., Herriott, R., Abdel-Rasoul, M., & Bolte, J. H. (2013). The response of pediatric ribs to quasi-static loading: mechanical properties and microstructure. *Annals of Biomedical Engineering*, *41*(12), 2501–2514.

Agnew, A. M., Schafman, M., Moorhouse, K., White, S. E., & Kang, Y.-S. (2015). The effect of age on the structural properties of human ribs. *Journal of the Mechanical Behavior of Biomedical Materials*, *41*, 302–314.

Baudrit, P., Petitjean, A., Potier, P., Trosseille, X., & Vallencien, G. (2014). Comparison of the thorax dynamic responses of small female and midsize male post mortem human subjects in side and forward oblique impact tests. *Stapp Car Crash Journal*, 58, 103-121.

Bergeron, E., Lavoie, A., Clas, D., Moore, L., Ratte, S., Tetreault, S., Lemaire, J., & Martin, M. (2003). Elderly trauma patients with rib fractures are at greater risk of death and pneumonia. *The Journal of Trauma*, *54*(3), 478–485.

Boskey, A. L., & Coleman, R. (2010). Aging and bone. *Journal of Dental Research*, 89 (12), 1333-1348.

Bulger, E. M., Arneson, M. A., Mock, C. N., & Jurkovich, G. J. (2000). Rib fractures in the elderly. *The Journal of Trauma*, *48*(6).

Charpail, E., Trosseille, X., Petit, P., Laporte, S., Lavaste, F., & Vallancien, G. (2005). Characterization of PMHS ribs: A new test methodology. *Stapp Car Crash Journal*, *49*, 183–198.

Cormier, J. M., Stitzel, J. D., Duma, S. M., & Matsuoka, F. (2005). Regional variation in the structural response and geometrical properties of human ribs. *Annual proceedings / Association for the Advancement of Automotive Medicine. Association for the Advancement of Automotive Medicine*, *49*, 153–170.

Fryar, C. D., Gu, Q., & Ogden, C. L. (2012). Anthropometric reference data for children and adults: United states, 2007-2010. *Vital and health statistics. Series 11, Data from the national health survey*, (252), 1–48.

Granik, G., & Stein, I. (1973). Human ribs: static testing as a promising medical application. *Journal of Biomechanics*, *6*(3), 237–240.

Holcomb, J. B., McMullin, N. R., Kozar, R. A., Lygas, M. H., & Moore, F. A. (2003). Morbidity from rib fractures increases after age 45. *Journal of the American College of Surgeons*, *196*(4), 549–555.

Holcombe, S. A., Wang, S. C., & Grotberg, J. B. (2016). Modeling female and male rib shapes with logarithmic spirals. *Journal of Biomechanics*, *49*(13), 2995–3003.

Kemper, A. R., McNally, C., Pullins, C. A., Freeman, L. J., Duma, S. M., & Rouhana, S. W. (2007). The biomechanics of human ribs: material and structural properties from dynamic tension and bending tests. *Stapp Car Crash Journal*, *51*, 235–273.

Kent, R., & Patrie, J. (2005). Chest deflection tolerance to blunt anterior loading is sensitive to age but not load distribution. *Forensic Science International*, *149*(2-3), 121–128.

Kent, R., Woods, W., & Bostrom, O. (2008). Fatality risk and the presence of rib fractures. *Annual Proceedings, Association for the Advancement of Automotive Medicine*, *52*, 73–82.

Kindig, M., Lau, A. G., & Kent, R. W. (2011). Biomechanical response of ribs under quasistatic frontal loading. *Traffic Injury Prevention*, *12*(4), 377–387.

Kindig, M. W., & Kent, R. W. (2013). Characterization of the centroidal geometry of human ribs. *Journal of Biomechanical Engineering, 135*(11).

Li, Z., Kindig, M. W., Kerrigan, J. R., Untaroiu, C. D., Subit, D., Crandall, J. R., & Kent, R. W. (2010). Rib fractures under anterior-posterior dynamic loads: experimental and finite-element study. *Journal of biomechanics*, *43*(2), 228–234.

Livingston, D. H., & Hauser, C. J. (2004). Trauma to the chest wall and lung. *Trauma*, 5.

Pintar, F. A., Yoganandan, N., Stemper, B. D., Bostrom, O., Rouhana, S. W., Digges, K. H., & Fildes, B. N. (2007). Comparison of PMHS, WorldSID, and THOR-NT responses in simulated far side impact. *Stapp Car Crash Journal, 51*, 313–360.

Shaw, J. M., Herriott, R. G., McFadden, J. D., Donnelly, B. R., & Bolte, J. H. (2006). Oblique and lateral impact response of the PMHS thorax. *Stapp Car Crash Journal, 50* , 147-167.

Shi, X., Cao, L., Reed, M. P., Rupp, J. D., Hoff, C. N., & Hu, J. (2014). A statistical human rib cage geometry model accounting for variations by age, sex, stature and body mass index. *Journal of Biomechanics*, *47*(10), 2277–2285.

Song, E., Trosseille, X., & Baudrit, P. (2009). Evaluation of thoracic deflection as an injury criterion for side impact using a finite elements thorax model. *Stapp Car Crash Journal, 53,* 155-191.

Stein, I. D. (1976). Rib structure and bending strength: an autopsy study. *Calcified tissue research*, *20*(1), 61–73.

Stitzel, J. D., Cormier, J. M., Barretta, J. T., Kennedy, E. A., Smith, E. P., Rath, A. L., Duma, S. M., & Matsuoka, F. (2003). Defining regional variation in the material properties of human rib cortical bone and its effect on fracture prediction. *Stapp car crash journal*, *47*, 243–265.

Takahashi, H., & Frost, H. M. (1966). Age and sex related changes in the amount of cortex of normal human ribs. *Acta Orthopaedica, 37*(2), 122–130.

Wang, Y., Cao, L., Bai, Z., Reed, M. P., Rupp, J. D., Hoff, C. N., & Hu, J. (2016). A parametric ribcage geometry model accounting for variations among the adult population. *Journal of Biomechanics*, *49*(13), 2791–2798.

APPENDIX

Table A1. Rib shape parameters by stiffness in free axial loading (5th, 50th, and 95th percentile stiffness across the population)

	S_x			X_{Pk}			Y_{Pk}			φ_{pia}			B_p			B_d		
Rib	5^{th}	50^{th}	95^{th}	5^{th}	50^{th}	95^{th}	5^{th}	50^{th}	95^{th}	5^{th}	50^{th}	95^{th}	5^{th}	50^{th}	95^{th}	5^{th}	50^{th}	95^{th}
1	73	71	65	0.40	0.40	0.41	0.60	0.52	0.47	82	80	78	-0.44	-0.48	-0.54	1.62	1.50	1.57
2	121	111	101	0.32	0.31	0.34	0.66	0.62	0.58	113	112	111	-0.28	-0.29	-0.40	0.72	0.65	0.92
3	150	142	132	0.34	0.34	0.35	0.63	0.59	0.54	114	117	121	-0.47	-0.50	-0.56	0.36	0.35	0.40
4	174	166	157	0.32	0.32	0.32	0.57	0.53	0.48	113	116	119	-0.44	-0.48	-0.56	-0.02	-0.10	0.02
5	194	185	176	0.32	0.31	0.31	0.52	0.48	0.44	111	115	117	-0.47	-0.51	-0.58	-0.28	-0.39	-0.43
6	205	199	190	0.31	0.30	0.28	0.48	0.43	0.39	109	114	116	-0.43	-0.45	-0.48	-0.46	-0.50	-0.51
7	217	207	201	0.30	0.29	0.27	0.44	0.40	0.34	106	111	114	-0.35	-0.36	-0.41	-0.34	-0.17	0.11
8	221	208	196	0.31	0.31	0.29	0.40	0.37	0.32	104	105	106	-0.32	-0.39	-0.43	-0.27	-0.22	-0.11
9	212	198	183	0.35	0.35	0.34	0.40	0.36	0.32	96	98	100	-0.47	-0.51	-0.65	-0.17	-0.06	0.00
10	200	182	165	0.38	0.37	0.37	0.38	0.33	0.29	88	88	85	-0.45	-0.54	-0.66	-0.07	-0.11	-0.15
11	180	154	132	0.39	0.39	0.41	0.32	0.28	0.23	85	82	77	-0.36	-0.58	-1.21	0.13	0.46	1.77
12	134	99	46	0.44	0.42	0.31	0.24	0.18	0.12	84	62	35	-1.29	-1.66	0.41	1.47	0.71	1.48

Table A2. Rib shape parameters by stiffness in constrained axial loading (5^{th}, 50^{th}, and 95^{th} percentile stiffness across the population)

	S_x			X_{Pk}			Y_{Pk}			φ_{pia}			B_p			B_d		
Rib	5^{th}	50^{th}	95^{th}	5^{th}	50^{th}	95^{th}	5^{th}	50^{th}	95^{th}	5^{th}	50^{th}	95^{th}	5^{th}	50^{th}	95^{th}	5^{th}	50^{th}	95^{th}
1	69	71	69	0.37	0.40	0.40	0.59	0.52	0.45	93	81	69	-0.51	-0.44	-0.45	2.24	1.63	1.95
2	113	110	108	0.27	0.32	0.37	0.68	0.62	0.56	118	112	105	-0.22	-0.29	-0.43	0.65	0.68	0.92
3	140	141	141	0.30	0.35	0.37	0.65	0.59	0.52	120	117	115	-0.41	-0.49	-0.61	0.36	0.38	0.47
4	164	167	166	0.29	0.32	0.35	0.58	0.53	0.48	119	115	113	-0.42	-0.50	-0.58	-0.04	-0.05	0.00
5	181	185	185	0.28	0.32	0.33	0.54	0.48	0.43	118	114	111	-0.42	-0.51	-0.56	-0.30	-0.37	-0.37
6	195	198	197	0.28	0.30	0.31	0.49	0.44	0.39	116	113	109	-0.41	-0.47	-0.46	-0.46	-0.51	-0.45
7	205	208	207	0.27	0.29	0.30	0.45	0.39	0.34	115	111	103	-0.35	-0.40	-0.34	-0.36	-0.22	0.21
8	211	207	204	0.29	0.31	0.31	0.41	0.36	0.32	109	107	97	-0.38	-0.41	-0.36	-0.35	-0.22	-0.09
9	206	199	190	0.34	0.35	0.35	0.40	0.35	0.31	103	99	92	-0.51	-0.56	-0.56	-0.23	-0.07	0.06
10	191	180	168	0.38	0.37	0.39	0.37	0.32	0.29	95	94	80	-0.67	-0.70	-0.55	0.07	-0.09	-0.10
11	173	149	134	0.39	0.38	0.39	0.31	0.27	0.23	96	83	73	-0.70	-0.69	-0.94	0.22	0.16	1.42
12	113	108	105	0.39	0.39	0.41	0.21	0.20	0.16	76	71	60	-0.66	-1.76	-2.00	2.50	0.97	0.58

Table A3. Rib shape parameters by stiffness in free lateral loading (5th, 50th, and 95th percentile stiffness across the population)

	S_x			X_{Pk}			Y_{Pk}			φ_{pia}			B_p			B_d		
Rib	5th	50th	95th	5th	50th	95th	5th	50th	95th	5th	50th	95th	5th	50th	95th	5th	50th	95th
1	80	70	63	0.41	0.38	0.28	0.52	0.51	0.51	76	79	92	-0.21	-0.39	-0.30	2.21	1.40	0.90
2	126	110	98	0.35	0.32	0.27	0.58	0.62	0.65	111	113	114	-0.44	-0.30	-0.14	0.98	0.71	0.49
3	162	141	125	0.36	0.34	0.32	0.53	0.59	0.63	117	117	119	-0.62	-0.49	-0.41	0.39	0.37	0.26
4	189	166	149	0.34	0.32	0.30	0.48	0.53	0.56	115	116	120	-0.63	-0.49	-0.41	-0.11	-0.04	-0.09
5	210	184	167	0.32	0.31	0.28	0.43	0.48	0.51	112	114	117	-0.66	-0.48	-0.38	-0.48	-0.39	-0.38
6	221	196	180	0.32	0.30	0.26	0.40	0.44	0.46	109	113	119	-0.64	-0.45	-0.28	-0.56	-0.53	-0.57
7	231	208	191	0.31	0.29	0.25	0.37	0.39	0.40	105	110	117	-0.58	-0.39	-0.27	-0.27	-0.24	-0.25
8	232	208	192	0.33	0.31	0.27	0.35	0.37	0.36	102	105	112	-0.56	-0.38	-0.28	-0.36	-0.17	-0.28
9	224	198	177	0.36	0.36	0.32	0.34	0.36	0.36	94	98	104	-0.65	-0.54	-0.48	-0.14	-0.06	-0.07
10	204	182	159	0.40	0.38	0.35	0.34	0.32	0.32	91	91	88	-0.77	-0.65	-0.39	-0.10	-0.21	-0.39
11	180	156	130	0.40	0.39	0.38	0.29	0.26	0.26	90	84	85	-0.63	-0.75	-0.84	-0.27	0.45	1.89
12	141	107	67	0.48	0.39	0.31	0.22	0.20	0.16	80	66	59	-1.74	-1.25	-0.50	2.40	0.30	1.25

Table A4. Rib shape parameters by stiffness in constrained lateral loading (5th, 50th, and 95th percentile stiffness across the population)

	S_x			X_{Pk}			Y_{Pk}			φ_{pia}			B_p			B_d		
Rib	5th	50th	95th	5th	50th	95th	5th	50th	95th	5th	50th	95th	5th	50th	95th	5th	50th	95th
1	71	77	72	0.43	0.33	0.44	0.60	0.51	0.59	86	78	72	-0.71	-0.24	0.43	2.50	2.50	0.86
2	117	111	103	0.28	0.32	0.35	0.64	0.63	0.59	121	113	103	-0.32	-0.30	-0.28	0.66	0.61	0.65
3	147	143	131	0.31	0.35	0.37	0.61	0.59	0.58	124	116	112	-0.48	-0.53	-0.49	0.38	0.38	0.31
4	177	167	154	0.30	0.33	0.34	0.54	0.52	0.52	121	117	110	-0.52	-0.52	-0.44	-0.07	0.03	-0.01
5	194	185	174	0.30	0.32	0.32	0.50	0.48	0.47	118	115	109	-0.56	-0.54	-0.41	-0.39	-0.31	-0.36
6	204	199	188	0.30	0.31	0.30	0.46	0.43	0.42	121	112	108	-0.57	-0.51	-0.26	-0.53	-0.56	-0.58
7	214	209	202	0.29	0.29	0.28	0.41	0.39	0.37	119	110	101	-0.60	-0.38	-0.16	-0.43	-0.12	0.01
8	222	208	197	0.31	0.31	0.30	0.37	0.36	0.34	112	105	96	-0.62	-0.39	-0.15	-0.47	-0.17	-0.12
9	215	197	182	0.36	0.35	0.34	0.36	0.36	0.34	105	97	92	-0.80	-0.55	-0.39	-0.35	-0.03	-0.01
10	197	179	167	0.35	0.37	0.37	0.31	0.33	0.34	91	91	78	-0.87	-0.50	-0.03	-0.19	-0.23	0.04
11	167	146	140	0.38	0.38	0.37	0.27	0.29	0.28	87	81	73	-0.97	-0.70	-0.05	-0.77	0.76	1.46
12	117	88	66	0.41	0.47	0.24	0.19	0.16	0.15	63	45	48	-1.88	-1.00	-0.17	0.98	1.28	2.50